Introduction

Most neurodegenerative conditions are characterized by the aggregation of a misfolded protein such as Aβ and tau in Alzheimer's disease (AD), transactive response (TAR) DNA binding protein 43 kDa (TDP-43) in some forms of frontotemporal lobar degeneration (FTLD) such as semantic dementia (SD) or α-synuclein in Parkinson's disease. Tauopathies are neurodegenerative diseases characterized by the pathological accumulation of aggregated tau. AD is the most common tauopathy and the leading cause of dementia [1], but tau deposits are also found in other variants of FTLD, such as progressive non-fluent aphasia (PNFA) or in some cases of behavioural frontotemporal dementia (bFTD) [2]. Other tauopathies include Down's syndrome, Guam parkinsonism-dementia complex, frontotemporal dementia with parkinsonism linked to chromosome 17, corticobasal degeneration, progressive supranuclear palsy and chronic traumatic encephalopathy [3–5]. Definitive diagnosis of these neurodegenerative conditions can only be established after death. While these tauopathies share tau immunoreactivity in post-mortem brain examination, these tau aggregates can be composed of different tau isoforms displaying very distinct histopathological and ultrastructural differences [3, 6, 7]. In AD, these tau deposits can be recognized histologically as neurofibrillary tangles (NFTs) and neuropil threads as well as dystrophic neurites in senile plaques, whilst ultrastructurally they aggregate in paired helical filaments (PHF) [3, 4, 8]. While the underlying mechanisms leading to tau hyperphosphorylation, misfolding and aggregation remain unclear, tau aggregation and deposition follows a stereotypical and spatiotemporal pathway both at the intraneuronal level [8, 9] as well as in its topographical and neuroanatomical distribution in the brain [4, 10, 11].

The notion that tau dysregulation is a key mediator of neurodegeneration [12, 13] has stimulated the development of therapeutics for the treatment of AD and non-AD tauopathies [14–16]. Given these treatments are currently being developed, a non-invasive method of determining the tau burden in the brain would allow a better understanding of the pathophysiology of AD, FTLD and other tau-related neurodegenerative conditions. It will also lead to improvements in differential diagnostic accuracy and accelerate drug discovery by facilitating patient selection and monitor efficacy in novel anti-tau therapeutic trials. It would assist in the early and differential diagnosis of AD and non-AD tauopathies, while helping ascertain the relationship between the spatiotemporal distribution of tau aggregates in the brain to cognition and brain volumetrics. Development of tau imaging probes poses several more challenges than those associated with Aβ imaging, and these are mainly related to the idiosyncrasies of tau aggregation and deposition. In contrast to Aβ, most tau aggregates are intracellular, there are six tau isoforms and the different combinations of these isoforms manifest as different clinical phenotypes. Tau aggregates undergo a wide spectrum of post-translation modifications that, in addition to the combination of different isoforms, lead to diverse ultrastructural conformations and typical pathological lesions. Furthermore, tau aggregates coexist with other misfolded proteins sharing the same β-sheet secondary structure, as is in the case of AD where tau and Aβ are both co-localized in grey matter areas, where the concentrations of Aβ are, depending on the brain region, ~5–20 times higher than those of tau (for an in depth review see Villemagne et al. [17]).

In recent years, the main focus has been the development of selective ligands that allow early detection of Aβ deposition [18]. Among these tracers, ^{18}F-FDDNP was reported to non-selectively bind to both Aβ deposits and NFTs [19]. Phenylquinoline derivatives binding with high affinity and selectivity for tau aggregates have been developed as candidates for tau imaging agents at Tohoku University in Sendai, Japan [20]. Among them, ^{18}F-THK523 (THK523) was the first reported selective tau imaging tracer that can non-invasively detect tau deposits in a transgenic mouse brain [21]. This report was recently followed by several other potential tau tracer candidates [22–27].

After a careful in vitro evaluation, the initial in vivo characterization of a novel positron emission tomography (PET) neuroligand candidate requires to fulfill certain conditions such as safety at low tracer doses, possess high affinity and selectivity for the target, ability to cross the blood–brain barrier, display low non-specific binding with adequate regional distribution and its relation to parameters known to be associated with the intended target, suitable brain kinetics, lack of problematic radiolabelled metabolites [28] before it is applied to research or clinical use (Supplementary Fig. 1).

Therefore, the main objective of the present study was to characterize the in vivo suitability of THK523 for tau imaging in humans. The in vivo assessment comprised: (a) comparing the global and regional THK523 binding in healthy controls (HC), AD and SD patients, (b) assessing the relationship between THK523 retention and cognition, (c) assessing the relationship between THK523 retention and brain volumetrics and (d) comparing the regional brain distribution of THK523 with that of ^{11}C-Pittsburgh compound B (PIB) in the same participants.

Materials and methods

Participants

Written informed consent was obtained from all participants. Approval for the study was obtained from the Austin Health Human Research Ethics Committee. Elderly HC were recruited by advertisement in the community and dementia patients

were recruited from tertiary Memory Disorders Clinics or from physicians who sub-specialize in dementia care. All participants were classified on the basis of their clinical and neuropsychological performance by consensus of a neurologist and a neuropsychologist. Individuals classified as HC performed within normal limits on cognitive tests. AD patients met NINCDS-ADRDA criteria for probable AD [29], while three FTLD patients were classified as SD [30, 31]. None of the AD or FTLD patients had a family history of dementia.

Safety evaluation

Clinical, haematological and biochemical data on the safety of THK523 were collected for all participants. Heart rate, blood pressure, temperature and respiratory rate were measured immediately prior to injection and at 2, 15, 60 and 180 min post-injection. Immediately prior to THK523 injection, blood was drawn for routine haematology and biochemistry tests. An ECG was performed prior to injection of THK523 and at the completion of the scan, when they were also questioned for adverse events. All subjects were contacted by telephone 24 h later and questioned for adverse events. Between 5 and 8 days post-injection, subjects returned to be questioned for adverse events and for a physical examination, including a set of observations and repeat haematology and biochemistry testing.

Neuropsychological evaluation

In addition to the Mini-Mental State Examination (MMSE), Clinical Dementia Rating (CDR) and Clinical Dementia Rating Sum of Boxes (CDR SOB), the primary cognitive performance measures were composite episodic memory and non-memory scores generated as previously described [32]. Briefly, a composite episodic memory score was calculated by taking the average of the z scores (generated using 65 HC with both low PIB and normal MRI as the reference) for Rey Complex Figure Test (RCFT, 30 min) Long Delay and California Verbal Learning Test - Second Edition (CVLT-II) Long Delay and Logical Memory II. A composite non-memory score was calculated by taking the average of the z scores for the Boston Naming Test, letter fluency, category fluency, digit span forwards and backwards, digit symbol-coding and RCFT copy.

Image acquisition

Magnetic resonance imaging

Participants received an MRI on a 3 T Siemens TRIO MRI system (Siemens Healthcare, Erlangen, Germany) using the Alzheimer's Disease Neuroimaging Initiative (ADNI) 3D magnetization prepared rapid acquisition gradient echo (MPRAGE) sequence with 1×1 mm in-plane resolution and 1.2-mm slice thickness, repetition time (TR)/echo time (TE)/T1-weighted=2,300/2.98/900, flip angle 9° and field of view 240×256 and 160 slices. T2 -weighted fast spin-echo (FSE) and fluid-attenuated inversion recovery (FLAIR) sequences were also obtained. The interval between the THK523 and MRI studies was 1.6±3.3 months.

Positron emission tomography

Productions of ^{11}C-PIB and ^{18}F-THK523 were performed in the Centre for PET, Austin Hospital. ^{11}C-PIB was synthesized using the one-step ^{11}C-methyl triflate approach as previously described [18]. The decay-corrected average radiochemical yield for ^{11}C-PIB was 30 % with a radiochemical purity of >98 % and a specific activity of 30±7. 5 GBq/μmol. ^{18}F-THK523 was synthesized by nucleophilic substitution of the tosylate precursor [BF-241, 2-3 mg in 700 μl dimethyl sulphoxide (DMSO)]. The decay-corrected average radiochemical yield of the production of ^{18}F-THK523 was 22.5± 5 %, with a radiochemical purity of>95 % and a specific activity of 225.6±134.8 GBq/μmol (6.2±3.3 Ci/μmol).

A 30-min acquisition (6×5-min frames) on an Allegro™ PET camera started 40 min after injection of 300 MBq ^{11}C-PIB intravenously. A 90-min list-mode emission acquisition was performed in 3D mode after injection of 200 MBq ^{18}F-THK523. List-mode raw data were sorted offline into 6×30-s, 7×1-min, 4×2.5-min, 2×5-min and 6×10-min frames. The sorted sinograms were reconstructed using a 3D row action maximum likelihood algorithm (RAMLA). The interval between the THK523 and PIB PET studies was 0.3±3.8 months.

Tracer metabolism

Compound stability was assessed by incubating the tracer for 5, 30, 60, 90, 180 and 240 min with human S9 liver fractions.

Image analysis

Magnetic resonance imaging

Hippocampal and cortical grey matter volumes were obtained using a commercial fully automated volumetric measurement program (NeuroQuant®) applied to the 3D MPRAGE MRI images. The primary MRI performance measures were the grey cortical matter and hippocampal volumes normalized for total intracranial volume.

Positron emission tomography

PET images were processed using a semi-automatic region of interest (ROI) method as previously described [32]. Briefly,

THK523 and PIB PET images were co-registered to each individual's MRI using SPM8 (Wellcome Trust Centre for Neuroimaging, London, UK), and the same ROI template was applied. Given the reversible nature of THK523 kinetics, distribution volume ratios (DVR) were determined through graphical analysis of the dynamic data. Standardized uptake value ratios (SUVR) for PIB and THK523 as well as THK523 DVR were generated using the cerebellar cortex as reference region [18, 33]. Global tau and Aβ burden were expressed as the average SUVR for the following cortical ROIs: frontal (consisting of dorsolateral prefrontal, ventrolateral prefrontal and orbitofrontal regions), superior parietal, lateral temporal, lateral occipital and anterior and posterior cingulate for THK523 and PIB, respectively. As in previous studies, a PIB SUVR threshold of 1.5 was used to categorize high (PIB+) and low (PIB−) Aβ burden [32].

Partial volume correction (PVC), accounting for *both* grey matter atrophy and white matter spillover, was performed applying a three-compartment approach using PMOD 3.1 (PMOD Technologies Ltd., Zurich, Switzerland). DVR for THK523 were determined through graphical analysis of the last 45 min of the 90-min acquisition [33]. In order to avoid arterial blood sampling, a simplified approach was applied using the cerebellar cortex as reference region [18, 33]. Global DVR was calculated with the same regions used for the global SUVR. The primary outcome measure used for all THK523 and PIB assessments was the PVC SUVR.

Statistical evaluation

Normality of distribution was tested using the Shapiro-Wilk test and visual inspection of variable histograms. Statistical evaluations to establish differences between clinical groups means were performed using a Tukey-Kramer HSD test and by a Dunnett's test to compare each group with controls. Pearson's product-moment correlation analyses were conducted between imaging and clinical variables. Categorical differences were evaluated using Fisher's exact test. Effect size was measured with Cohen's *d*. All analyses were adjusted for age and corrected for multiple comparisons using false discovery rates. Data are presented as mean±standard deviation unless otherwise stated.

Results

Participants

Demographic characteristics of the participants are shown in Table 1. As expected, there were significant differences between the AD and SD patients and HC in cognitive performance and brain volumetrics. The AD group also presented with significantly higher PIB retention. While there were no significant differences between groups in age and gender, the AD group was less educated. While seven of the HC and the three SD patients showed low PIB retention, three of the HC presented with high PIB retention (Table 1).

No adverse events related to the study drug were observed or reported by participants or carers following the THK523 scan. There were no significant changes in clinical or biochemical parameters.

Tracer metabolism

THK523 was minimally metabolized, with 91, 81 and 65 % of unchanged parent compound remaining at 30, 90 and 180 min, respectively. No lipophilic radiometabolites were observed.

Brain kinetics

Brain THK523 radioactivity peaked between 3 and 6 min post-injection and the binding appeared to be reversible with rapid clearance from the brain (Fig. 1a, b). THK523 cleared fastest from cerebellar cortex and the clearance rate was the same for all groups (Fig. 1a, b). Clearance was slower from cortical areas in AD (Fig. 1b) than in HC (Fig. 1a) and SD patients. The ratio of cortical to cerebellar binding became constant in all participants by 50 min after injection (Fig. 1c).

Visual inspection

Visual inspection of the summed 60–90-min SUVR images revealed significantly higher THK523 retention in white matter than in grey matter regions, being significantly higher in AD patients than in HC or SD (Fig. 1d).

Assessment of tau burden

Regional analysis showed that there were no group differences in cerebellar cortex THK523 SUV, and there was no correlation between cerebellar cortex THK523 SUV with age in the whole cohort or with dementia severity in the AD group as assessed by MMSE (r=0.25, p=0.50), CDR (r=0.13, p=0.72) or CDR SOB (r=0.03, p=0.94).

While 60–90-min THK523 SUVR was estimated for all participants, four participants (two HC and two AD) were not able to complete the initial THK523 dynamic scan preventing calculation of DVR. In the remaining 16 subjects, significantly higher THK523 DVR were found in AD subjects in all cortical regions. The global THK523 DVR was 1.02±0.15 in AD vs 0.86±0.11 in HC (p=0.04, Cohen's effect size d=1.2). No significant differences were observed between HC and SD patients. Similar findings were observed with THK523

Table 1 Demographics

	HC (n=10)	SD (n=3)	AD (n=10)
Age	77.4±10.0	65.6±8.1	75.6±9.5
Gender (M/F)	3/7	1/2	4/6
MMSE	29.3±1.1	21.7±1.2*	16.7±6.6*
CDR	0.0	0.8±0.3*	1.3±0.6*
CDR SOB	0.1±0.2	2.5±1.1*	7.3±4.5*
Years of education	14.7±2.7	12.5±4.9	11.5±3.6*
Episodic memory scores	−0.4±0.6	−1.9±0.9*	−3.8±0.5*
Non-memory scores	−0.1±0.4	−1.4±1.2*	−3.4±1.6*
Hippocampal volume (cm^3)	5.1±0.6	4.3±0.3	4.1±1.0*
Aβ burden (PIB SUVR)	1.5±0.6	1.1±0.1	2.9±0.5*
	[PIB−=1.2±0.1 (n=7)]		
	[PIB+=2.2±0.6 (n=3)]		

MMSE Mini-Mental State Examination, *CDR* Clinical Dementia Rating, *CDR SOB* Clinical Dementia Rating Sum of Boxes, *PIB* Pittsburgh compound B, *SUVR* standardized uptake value ratio, *PIB−* low PIB retention, *PIB+* high PIB retention

*Significantly different from HC (p<0.05)

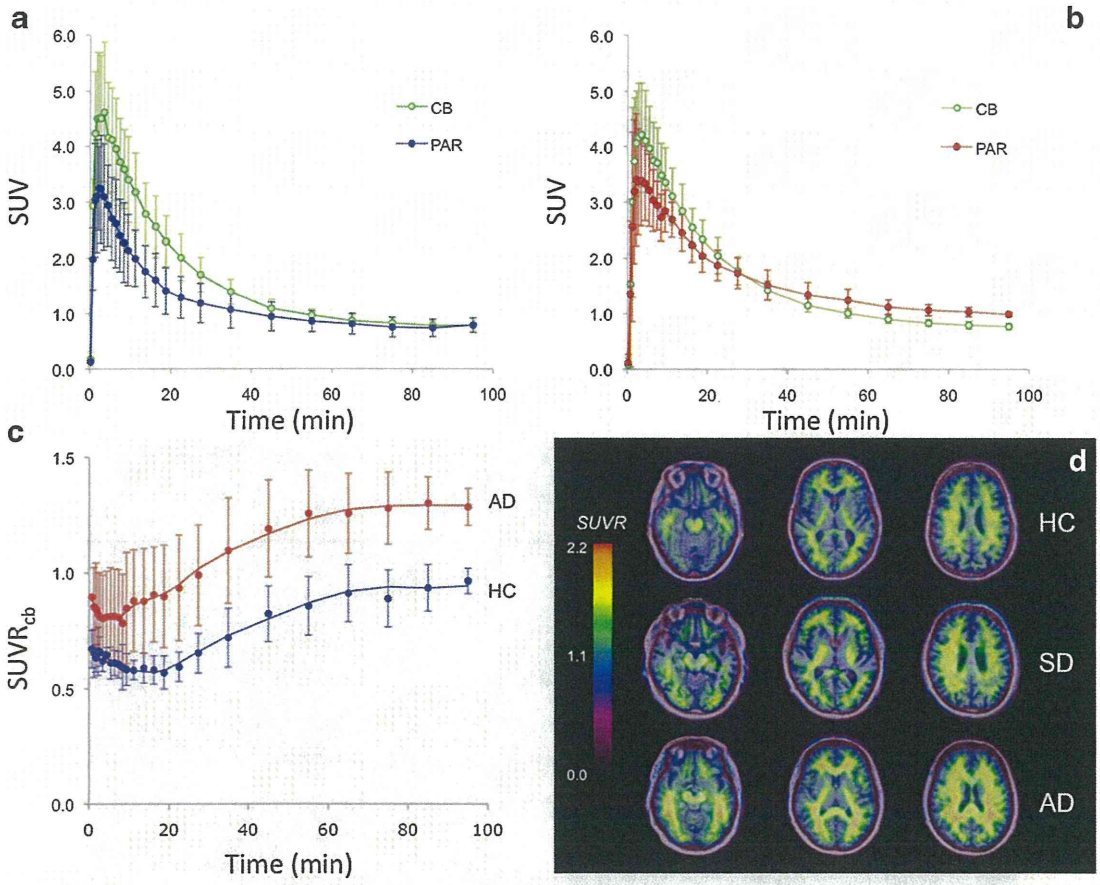

Fig. 1 ^{18}F-THK523 binding. Time-radioactivity curves for ^{18}F-THK523 in the parietal cortex (*PAR*) and the cerebellar grey matter (*CB*) in healthy controls (*HC*) (**a**) and Alzheimer's disease (*AD*) patients (**b**). There is fast ^{18}F-THK523 uptake in the brain followed by a fast clearance phase. While there is slower clearance with significantly higher retention in the parietal cortex of AD patients compared to HC, there are no significant differences in the cerebellar cortex uptake and clearance, further validating its use as reference region. **c** The total to non-specific binding ratios curves show significantly higher ^{18}F-THK523 retention in the parietal cortex of AD patients compared to HC. The specific binding reaches a plateau by 50 min post-injection. **d** Representative ^{18}F-THK523 PET images at three different brain levels in a 69-year-old female HC (MMSE 30, *top row*), a 73-year-old male semantic dementia (*SD*) patient (MMSE 21, *middle row*) and a 72-year-old female AD patient (MMSE 22, *bottom row*). Visual inspection of the images reveals no differences in ^{18}F-THK523 retention between HC and SD. There is higher white matter retention in AD compared to HC and SD. Data expressed as mean±SD of ten HC and ten AD patients

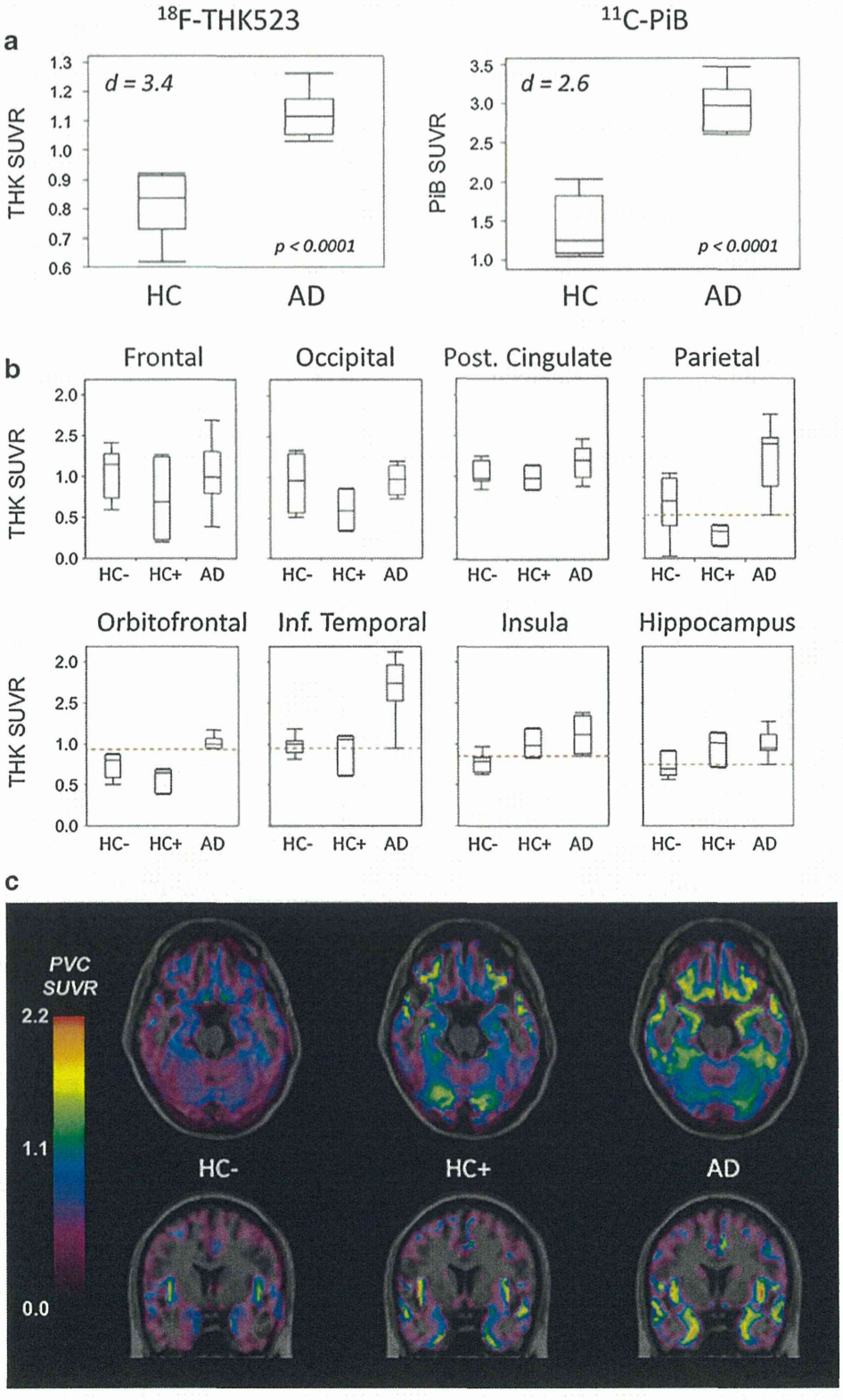

SUVR, and although SUVR values were higher than THK523 DVR, the rank order of the participants and the rank order of the regional values were identical, both showing the highest THK523 retention in temporal, parietal and hippocampus.

Table 2 Global and regional ^{18}F-THK523 and ^{11}C-PIB retention in AD

Region	THK SUVR				PIB SUVR			
	HC	AD	*p*	*d*	HC	AD	*p*	*d*
Frontal lobe	0.92±0.38	1.01±0.36	0.56	0.24	1.51±0.74	3.05±0.68	<0.0001	2.17
Orbitofrontal	0.68±0.16	1.06±0.24	<0.0001	1.87	1.42±0.50	2.91±0.58	<0.0001	2.74
Ant. cingulate	0.60±0.45	0.54±0.22	0.52	−0.19	1.61±0.75	2.98±0.59	<0.0001	2.04
Post. Cingulate	0.99±0.15	1.17±0.20	0.029	1.02	1.57±0.65	3.39±0.49	<0.0001	3.16
Parietal lobe	0.54±0.33	1.24±0.38	<0.0001	1.99	1.33±0.63	2.77±0.45	<0.0001	2.63
Lat. occipital lobe	0.81±0.33	0.91±0.29	0.38	0.31	1.35±0.35	2.32±0.38	<0.0001	2.66
Sup. temporal lobe	0.94±0.37	1.35±0.29	0.005	1.22	1.46±0.65	2.83±0.61	<0.0001	2.17
Inf. temporal lobe	0.96±0.16	1.81±0.58	<0.0001	2.00	1.52±0.62	2.89±0.51	<0.0001	2.42
Hippocampus	0.78±0.18	0.97±0.18	0.008	1.01	1.53±0.31	1.82±0.32	0.08	0.93
Insula	0.85±0.16	1.09±0.22	0.007	1.30	1.54±0.48	2.35±0.38	<0.0001	1.87
Striatum	0.39±0.16	0.46±0.25	0.65	0.33	1.79±0.76	2.98±0.64	0.0004	1.71
Subcortical white matter[a]	1.61±0.12	1.90±0.17	0.002	2.01	2.14±0.28	2.41±0.37	0.10	0.83
Neocortical	0.82±0.10	1.13±0.07	<0.0001	3.42	1.46±0.61	2.88±0.48	<0.0001	2.59

All images were partial volume corrected and then scaled and sampled. All results are adjusted for age
HC healthy control, *AD* Alzheimer's disease, *THK* ^{18}F-THK523, *PIB* ^{11}C-Pittsburgh compound B, *SUVR* standardized uptake value ratio, *d* Cohen's effect size *d*
[a] White matter SUVR are not partial volume corrected

THK523 SUVR correlated strongly with THK523 DVR in all cortical regions with a correlation coefficient of $r=0.85$ ($p<0.0001$) for the mean global measure.

Regional analysis of the non-partial volume-corrected images revealed significantly higher cortical THK523 retention in AD (Supplementary Fig. 2a) than in HC and SD patients. THK523 retention was also significantly higher in subcortical white matter in AD (Table 2). The spillover from the high retention in white matter was likely to contribute substantially to the radioactivity measured in grey matter; therefore, PVC of the images, correcting for *both* cortical grey matter atrophy and for white matter spillover, was performed. The PVC SUVR derived from the summed 60–90 min were subsequently used to assess THK523 retention as well as comparison with PIB and for correlation with brain volumetrics and cognitive parameters (Table 2). After PVC, while little or no THK523 retention was observed in cortical areas in HC, THK523 retention in AD patients was most prominent in cortical association areas, where only the temporal, parietal, hippocampal, orbitofrontal, and posterior cingulate regions (Supplementary Fig. 2b), brain areas known from post-mortem studies to contain substantial amounts of tau deposits in AD [10, 11], remained significant (Table 2). No significant differences were observed between HC and SD patients using either THK523 (Supplementary Table 1) or PIB (Supplementary Table 2). Global THK523 PVC SUVR in HC was 0.82±0.10 compared to 1.13±0.07 in AD ($p<0.0001$, Cohen's $d=3.4$) (Fig. 2).

Comparison of THK523 and PIB cortical retention

While seven of the ten HC and the three SD patients showed low Aβ burdens, all the AD patients and three HC presented with high Aβ burdens in the brain. In AD patients, the topographical pattern of cortical THK523 retention was clearly different from the cortical retention observed with PIB. While PIB was highest in the frontal, posterior cingulate, striatum and temporal cortices, THK523 was highest in temporal, parietal, hippocampus and posterior cingulate (Supplementary Fig. 3a). There was no correlation between the cortical THK523 SUVR and cortical PIB SUVR in the AD patients ($r=0.04$, $p=0.90$) (Supplementary Fig. 3b). Interestingly, in those HC with high Aβ burden (PIB+HC) while cortical THK523 retention was not significantly different to the cortical retention in PIB− HC, THK523 retention in the

◀ **Fig. 2** Global and regional retention of ^{18}F-THK523 and ^{11}C-PIB in AD. **a** Box plots for ^{18}F-THK523 (*left top panel*) and ^{11}C-PIB (*right top panel*) showing the global SUVR of both tracers. **b** When cognitively unimpaired HC with high (*HC+*) or low (*HC–*) ^{11}C-PIB retention were examined separately, it was observed that while ^{18}F-THK523 retention in isocortex of individuals with high ^{11}C-PIB retention aligned with those with low ^{11}C-PIB retention ^{18}F-THK523 retention in hippocampus and insula were not significantly different from the ^{18}F-THK523 retention in AD. *Red dotted lines* denote the bottom quartile of THK523 SUVR in AD patients. **c** Average parametric ^{18}F-THK523 transaxial and coronal partial volume-corrected (*PVC*) PET images overlaid on MRI of ten HC and ten AD patients, showing higher hippocampal and insular ^{18}F-THK523 retention on three HC with high (*HC+*) ^{11}C-PIB retention compared with seven HC with low (*HC–*) ^{11}C-PIB retention

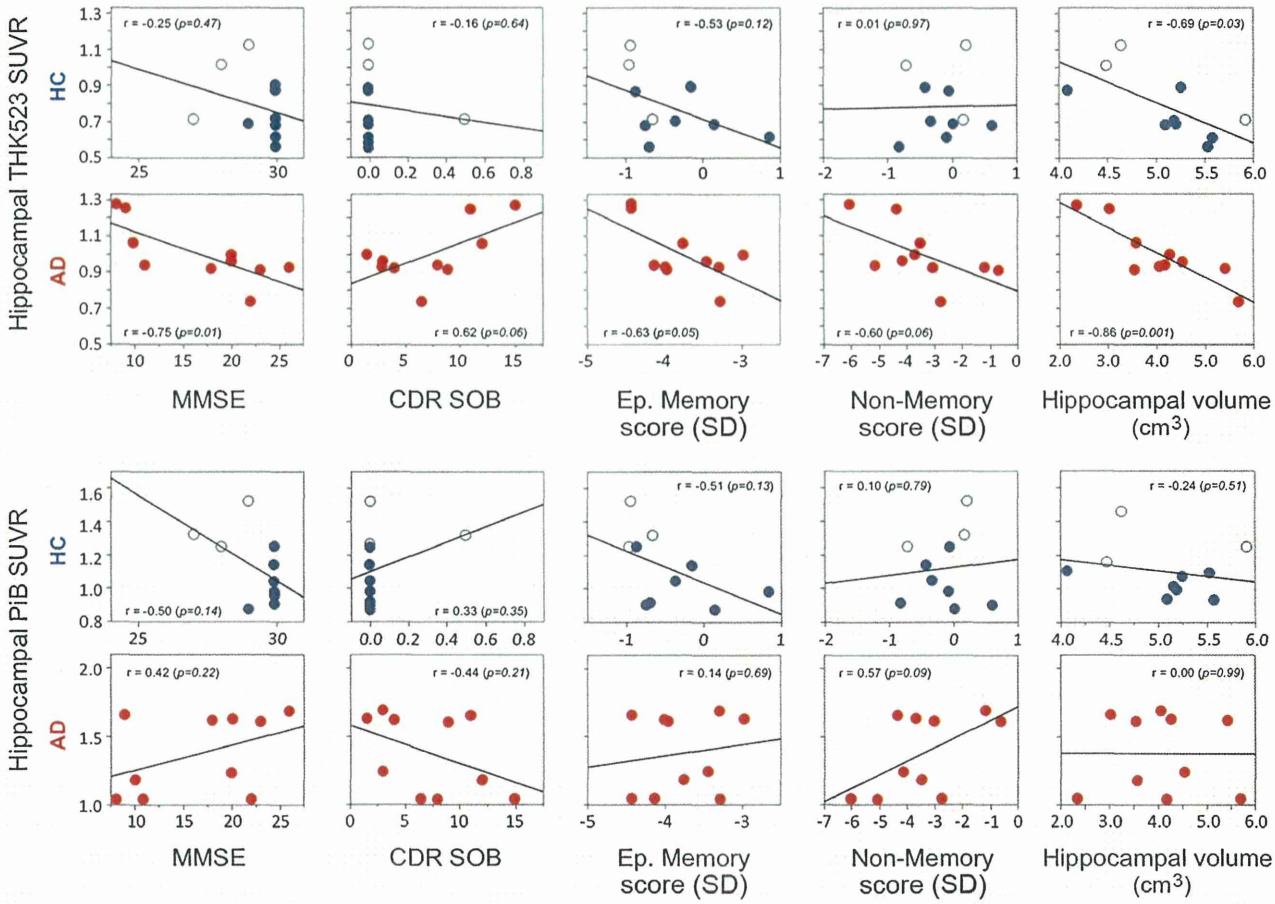

Fig. 3 Relationship between hippocampal ^{18}F-THK523 and ^{11}C-PIB retention with cognition and hippocampal volume. Regression analysis shows that while hippocampal ^{18}F-THK523 retention is not associated with cognition in HC, it is strongly associated with different cognitive parameters in AD patients (*top two rows*). On the other hand, hippocampal ^{18}F-THK523 retention is strongly associated with hippocampal volume in both HC and AD patients. There was no association between hippocampal ^{11}C-PIB retention (*bottom two rows*) with either cognitive parameters or hippocampal volume in any of the groups examined. All correlations were adjusted for age

hippocampus and insula was significantly higher than PIB–HC, but not significantly different from AD (Fig. 2).

Association between THK523 retention, cognition and brain volumetrics

While providing evidence of the general direction of the association between the different parameters (e.g. higher tau burden, lower cognitive performance), the associations derived from assessing all groups together tend to yield spurious correlations driven by the significant differences between the clinical groups. In order to avoid this issue, the associations with cognition and brain volumetrics were assessed in each clinical group separately.

In the case of THK523, there were no associations between cortical THK523 retention and cognitive parameters in HC, with the exception of the insula associated with episodic memory scores (r=−0.70, p=0.026). In the AD group, hippocampal THK523 retention was significantly associated with MMSE (r=−0.75, p=0.01) and episodic memory (r=−0.63, p=0.05) (Fig. 3). In the AD group, a strong trend was also observed between hippocampal THK523 retention, CDR SOB (r=0.62, p=0.055) and non-memory scores (r=−0.60, p=0.056). In regard to brain volumes, only hippocampal THK523 retention was significantly associated with hippocampal volume in both the HC (r=−0.69, p=0.03) and AD (r=−0.86, p=0.001) groups (Fig. 3). There were no correlations between global THK523 retention and cortical grey matter volume in any of the groups.

In the case of PIB, there were associations between PIB retention and MMSE in the orbitofrontal (r=−0.67, p=0.034), anterior (r=−0.65, p=0.04) and posterior cingulate (r=−0.78, p=0.007) regions of HC. In AD, there were some associations between PIB retention and cognitive parameters, but these correlations were, in every case, in the opposite direction as expected, where PIB retention in the anterior cingulate gyrus was positively associated with MMSE (r=0.63, p=0.049),

episodic memory (r=0.73, p=0.016) and non-memory scores (r=0.64, p=0.046) and inversely associated with CDR SOB (r=−0.68, p=0.03). There were no associations between hippocampal PIB retention and any cognitive parameter in any of the clinical groups (Fig. 3). There were no significant associations between global PIB retention and cortical grey matter volume in either HC or AD patients. In contrast to what was observed for hippocampal THK523 retention, there was no association between hippocampal PIB retention and hippocampal volume in any of the groups examined (Fig. 3).

Discussion

To the best of our knowledge, this is the first time a selective tau imaging agent has been thoroughly evaluated in human volunteers, assessing its associations with cognition and brain volumetrics, as well as a direct comparison with Aβ imaging using PIB.

Global cortical THK523 binding provided a very robust separation of AD patients from healthy elderly subjects (Cohen's d=3.4). Furthermore, cortical THK523 retention in AD patients followed the reported histopathological brain distribution of PHF-tau in AD [10, 11]. Examination of the brain kinetics of THK523 showed that it presents reversible binding kinetics, reaching apparent steady state about 50 min after injection of the radiotracer. Visual inspection of the THK523 images was hampered by the very high retention in white matter. In addition to the high non-specific binding, previous reports have demonstrated substantial concentrations of PHF-tau in white matter in AD [34, 35], suggesting THK523 retention in white matter might not solely reflect marked non-specific binding, but also some small degree of specific binding. Several factors were taken into account for the selection of the reference region. To date, no report has described tau deposition in the cerebellar cortex in sporadic AD [36]. There were no group differences in cerebellar cortex THK523 SUV, and there was no association between cerebellar cortex THK523 SUV with age in the whole cohort, or with dementia severity in the AD group, further supporting the use of the cerebellar cortex as reference region.

The regional brain distribution of THK523 showed a marked contrast when compared to that of PIB. While the highest PIB retention was observed in frontal, posterior cingulate, caudate and temporal cortices, the highest THK523 retention was observed in the inferior temporal, orbitofrontal, hippocampus, insula and parietal cortices. This was further confirmed by a lack of correlation between PIB SUVR and THK523 SUVR (r=0.04, p=0.90).

SD patients were included in the evaluation of THK523 as pathological controls [31]. Rather than tau aggregates, the vast majority of SD cases have been associated with the aggregation of TDP-43 [2, 31]. SD patients showed neither THK523 nor PIB retention in the brain (Supplementary Tables 1 and 2), suggesting the absence of both Aβ [37] and tau deposits in SD.

Three HC showed high cortical PIB retention (PIB+HC), consistent with previous PIB studies that have reported positive scans in 25–35 % of normal elderly individuals [38]. Despite the limited subsample size the finding is interesting because while cortical THK523 retention in PIB+HC was not significantly different from the cortical retention in PIB− HC, THK523 retention in the hippocampus and insula was significantly higher than in PIB− HC, but not significantly different from AD, suggesting that tau deposition in these regions might precede the dementia of AD [6, 39]. These findings might indicate that the combination of widespread cortical Aβ plus hippocampal tau deposition might not be enough to lead to significant cognitive impairment, requiring tau deposition in polymodal and unimodal association areas of the brain for objective cognitive impairment to be manifest [7, 10, 11].

As with Aβ imaging [40], longitudinal studies will assist in establishing the spatiotemporal patterns of tau deposition and help determine whether or not apparently healthy individuals with substantial hippocampal tau deposition will develop the AD phenotype, thus allowing very early, even preclinical diagnosis of AD, or if hippocampal tau deposits are just an age-associated process and only cortical tau deposition leads to cognitive impairment [39, 41].

In AD, hippocampal THK523 retention was associated with cognitive parameters. Similarly, hippocampal THK523 retention was associated with hippocampal volume in both HC and AD patients. Human post-mortem studies have shown that the density of NFTs strongly correlates with neurodegeneration and cognitive deficits, while Aβ plaque density does not [42, 43], a finding that was further confirmed through Aβ imaging studies [18, 32]. Furthermore, in stark contrast with Aβ plaques, NFTs are usually not present in associating cortical regions in cognitively unimpaired individuals [11, 18, 39].

As was previously reported in vitro [21, 44], several lines of evidence support the notion that THK523 selectively binds to PHF-tau and not to Aβ in vivo: (a) cortical THK523 retention is significantly higher in AD, following the known distribution of PHF-tau in the AD brain; (b) PIB and THK523 show different brain regional distribution patterns; (c) there is no correlation between PIB and THK523 retention; and (d) while hippocampal THK523 retention significantly correlates with cognitive parameters and hippocampal atrophy, hippocampal PIB retention does not.

While this was a first-in-human study, the limited sample size requires cautious interpretation of the findings. Furthermore, while our results suggest that ^{18}F-THK523 can reliably quantify PHF-tau deposition in vivo, there are serious limitations associated with the tracer itself. The high white matter THK523 retention, even if it might reflect some small degree of specific binding, precludes simple visual inspection of the

images and requires additional careful PVC even for a simple semi-quantitative analysis, preventing the use of THK523 in research or clinical settings.

Conclusion

This study has shown that despite selective, non-invasive in vivo assessment of PHF-tau in humans being possible, a single aspect of the in vivo behaviour of a tracer can derail its further development. This highlights the need for careful in vivo proof of concept studies at the initial stages of the development before embarking on more complex quantification approaches involving invasive procedures such as arterial cannulation or engaging in costly phase II studies. Better tau tracers, some of them already being evaluated in humans [23, 25–27], will be required for applications such as monitoring disease progression and assessing efficacy of anti-tau therapy. The development of ^{18}F-THK523 has shown to be a significant step towards the integration of tau imaging with Aβ imaging, moving us towards meeting the desired goal of earlier diagnosis of AD to assist the development of preventative treatments as well as identifying subjects for early therapeutic interventions.

Acknowledgements We thank Prof. Michael Woodward, Dr. John Merory, Dr. Gordon Chan, Dr. Kenneth Young, Dr. David Darby, Ms. Fiona Lamb and the Brain Research Institute for their assistance with this study. The study was partially supported by an Alzheimer Drug Discovery Foundation Research Grant (20101208 AFTD) and by a National Health and Medical Research Council of Australia Project Grant 1044361. The funding sources had no input into the design and conduct of the study; collection, management, analysis and interpretation of the data; and in the preparation, review, approval or decision to submit the manuscript for publication.

Conflicts of interest None.

References

1. Masters CL, Cappai R, Barnham KJ, Villemagne VL. Molecular mechanisms for Alzheimer's disease: implications for neuroimaging and therapeutics. J Neurochem 2006;97(6):1700–25. doi:10.1111/j.1471-4159.2006.03989.x.
2. Rabinovici GD, Miller BL. Frontotemporal lobar degeneration: epidemiology, pathophysiology, diagnosis and management. CNS Drugs 2010;24(5):375–98. doi:10.2165/11533100-000000000-00000.
3. Mohorko N, Bresjanac M. Tau protein and human tauopathies: an overview. Zdrav Vestn 2008;77(Suppl II):35–41.
4. Komori T. Tau-positive glial inclusions in progressive supranuclear palsy, corticobasal degeneration and Pick's disease. Brain Pathol 1999;9(4):663–79.
5. McKee AC, Cantu RC, Nowinski CJ, Hedley-Whyte ET, Gavett BE, Budson AE, et al. Chronic traumatic encephalopathy in athletes: progressive tauopathy after repetitive head injury. J Neuropathol Exp Neurol 2009;68(7):709–35. doi:10.1097/NEN.0b013e3181a9d503.
6. Delacourte A. Tauopathies: recent insights into old diseases. Folia Neuropathol 2005;43(4):244–57.
7. Buée L, Bussière T, Buée-Scherrer V, Delacourte A, Hof PR. Tau protein isoforms, phosphorylation and role in neurodegenerative disorders. Brain Res Brain Res Rev 2000;33(1):95–130.
8. Mandelkow E, von Bergen M, Biernat J, Mandelkow EM. Structural principles of tau and the paired helical filaments of Alzheimer's disease. Brain Pathol 2007;17(1):83–90. doi:10.1111/j.1750-3639.2007.00053.x.
9. Braak H, Braak E. Evolution of neuronal changes in the course of Alzheimer's disease. J Neural Transm Suppl 1998;53:127–40.
10. Braak H, Braak E. Staging of Alzheimer's disease-related neurofibrillary changes. Neurobiol Aging 1995;16(3):271–8. discussion 278–84.
11. Delacourte A, David JP, Sergeant N, Buée L, Wattez A, Vermersch P, et al. The biochemical pathway of neurofibrillary degeneration in aging and Alzheimer's disease. Neurology 1999;52(6):1158–65.
12. Goedert M, Jakes R. Mutations causing neurodegenerative tauopathies. Biochim Biophys Acta 2005;1739(2–3):240–50.
13. Roberson ED, Scearce-Levie K, Palop JJ, Yan F, Cheng IH, Wu T, et al. Reducing endogenous tau ameliorates amyloid beta-induced deficits in an Alzheimer's disease mouse model. Science 2007;316(5825):750–4.
14. Wischik CM, Edwards PC, Lai RY, Roth M, Harrington CR. Selective inhibition of Alzheimer disease-like tau aggregation by phenothiazines. Proc Natl Acad Sci U S A 1996;93(20):11213–8.
15. Brunden KR, Zhang B, Carroll J, Yao Y, Potuzak JS, Hogan AM, et al. Epothilone D improves microtubule density, axonal integrity, and cognition in a transgenic mouse model of tauopathy. J Neurosci 2010;30(41):13861–6. doi:10.1523/JNEUROSCI.3059-10.2010.
16. Bulic B, Pickhardt M, Mandelkow EM, Mandelkow E. Tau protein and tau aggregation inhibitors. Neuropharmacology 2010;59(4–5):276–89. doi:10.1016/j.neuropharm.2010.01.016.
17. Villemagne VL, Furumoto S, Fodero-Tavoletti MT, Harada R, Mulligan RS, Kudo T, et al. The challenges of tau imaging. Future Neurol 2012;7(4):409–21.
18. Rowe CC, Ng S, Ackermann U, Gong SJ, Pike K, Savage G, et al. Imaging beta-amyloid burden in aging and dementia. Neurology 2007;68(20):1718–25. doi:10.1212/01.wnl.0000261919.22630.ea.
19. Small GW, Kepe V, Ercoli LM, Siddarth P, Bookheimer SY, Miller KJ, et al. PET of brain amyloid and tau in mild cognitive impairment. N Engl J Med 2006;355(25):2652–63.
20. Okamura N, Suemoto T, Furumoto S, Suzuki M, Shimadzu H, Akatsu H, et al. Quinoline and benzimidazole derivatives: candidate probes for in vivo imaging of tau pathology in Alzheimer's disease. J Neurosci 2005;25(47):10857–62.
21. Fodero-Tavoletti MT, Okamura N, Furumoto S, Mulligan RS, Connor AR, McLean CA, et al. 18F-THK523: a novel in vivo tau imaging ligand for Alzheimer's disease. Brain 2011;134(Pt 4):1089–100. doi:10.1093/brain/awr038.
22. Zhang W, Arteaga J, Cashion DK, Chen G, Gangadharmath U, Gomez LF, et al. A highly selective and specific PET tracer for imaging of tau pathologies. J Alzheimers Dis 2012;31(3):601–12. doi:10.3233/JAD-2012-120712.
23. Chien DT, Bahri S, Szardenings AK, Walsh JC, Mu F, Su MY, et al. Early clinical PET imaging results with the novel PHF-tau radioligand [F-18]-T807. J Alzheimers Dis 2013;34(2):457–68. doi:10.3233/JAD-122059.
24. Shao XM, Carpenter GM, Desmond TJ, Sherman P, Quesada CA, Fawaz M, et al. Evaluation of [11C]N-methyl lansoprazole as a radiopharmaceutical for PET imaging of tau neurofibrillary tangles. ACS Med Chem Lett 2012;3(11):936–41.
25. Okamura N, Furumoto S, Harada R, Tago T, Yoshikawa T, Fodero-Tavoletti M, et al. Novel 18F-labeled arylquinoline derivatives for noninvasive imaging of tau pathology in Alzheimer disease. J Nucl Med 2013;54(8):1420–7. doi:10.2967/jnumed.112.117341.

26. Maruyama M, Shimada H, Suhara T, Shinotoh H, Ji B, Maeda J, et al. Imaging of tau pathology in a tauopathy mouse model and in Alzheimer patients compared to normal controls. Neuron 2013;79(6):1094–108. doi:10.1016/j.neuron.2013.07.037.
27. Chien DT, Szardenings AK, Bahri S, Walsh JC, Mu F, Xia C, et al. Early clinical PET imaging results with the novel PHF-tau radioligand [F18]-T808. J Alzheimers Dis 2014;38:171–84. doi:10.3233/JAD-130098.
28. Pike VW. PET radiotracers: crossing the blood–brain barrier and surviving metabolism. Trends Pharmacol Sci 2009;30(8):431–40. doi:10.1016/j.tips.2009.05.005.
29. McKhann G, Drachman D, Folstein M, Katzman R, Price D, Stadlan EM. Clinical diagnosis of Alzheimer's disease: report of the NINCDS-ADRDA Work Group under the auspices of Department of Health and Human Services Task Force on Alzheimer's Disease. Neurology 1984;34:939–44.
30. McKhann GM, Albert MS, Grossman M, Miller B, Dickson D, Trojanowski JQ, et al. Clinical and pathological diagnosis of frontotemporal dementia: report of the Work Group on Frontotemporal Dementia and Pick's Disease. Arch Neurol 2001;58(11):1803–9.
31. Hodges JR, Patterson K. Semantic dementia: a unique clinicopathological syndrome. Lancet Neurol 2007;6(11):1004–14.
32. Villemagne VL, Pike KE, Chételat G, Ellis KA, Mulligan RS, Bourgeat P, et al. Longitudinal assessment of Aβ and cognition in aging and Alzheimer disease. Ann Neurol 2011;69(1):181–92. doi:10.1002/ana.22248.
33. Price JC, Klunk WE, Lopresti BJ, Lu X, Hoge JA, Ziolko SK, et al. Kinetic modeling of amyloid binding in humans using PET imaging and Pittsburgh Compound-B. J Cereb Blood Flow Metab 2005;25(11):1528–47.
34. Mukaetova-Ladinska EB, Harrington CR, Roth M, Wischik CM. Biochemical and anatomical redistribution of tau protein in Alzheimer's disease. Am J Pathol 1993;143(2):565–78.
35. Khatoon S, Grundke-Iqbal I, Iqbal K. Levels of normal and abnormally phosphorylated tau in different cellular and regional compartments of Alzheimer disease and control brains. FEBS Lett 1994;351(1):80–4.
36. Larner AJ. The cerebellum in Alzheimer's disease. Dement Geriatr Cogn Disord 1997;8(4):203–9.
37. Rabinovici GD, Jagust WJ, Furst AJ, Ogar JM, Racine CA, Mormino EC, et al. Abeta amyloid and glucose metabolism in three variants of primary progressive aphasia. Ann Neurol 2008;64(4):388–401.
38. Rowe CC, Ellis KA, Rimajova M, Bourgeat P, Pike KE, Jones G, et al. Amyloid imaging results from the Australian Imaging, Biomarkers and Lifestyle (AIBL) study of aging. Neurobiol Aging 2010;31(8):1275–83. doi:10.1016/j.neurobiolaging.2010.04.007.
39. Delacourte A, Sergeant N, Wattez A, Maurage CA, Lebert F, Pasquier F, et al. Tau aggregation in the hippocampal formation: an ageing or a pathological process? Exp Gerontol 2002;37(10–11):1291–6.
40. Villemagne VL, Burnham S, Bourgeat P, Brown B, Ellis KA, Salvado O, et al. Amyloid beta deposition, neurodegeneration, and cognitive decline in sporadic Alzheimer's disease: a prospective cohort study. Lancet Neurol 2013;12(4):357–67. doi:10.1016/S1474-4422(13)70044-9.
41. Price JL, Morris JC. Tangles and plaques in nondemented aging and "preclinical" Alzheimer's disease. Ann Neurol 1999;45(3):358–68.
42. Arriagada PV, Growdon JH, Hedley-Whyte ET, Hyman BT. Neurofibrillary tangles but not senile plaques parallel duration and severity of Alzheimer's disease. Neurology 1992;42(3 Pt 1):631–9.
43. McLean CA, Cherny RA, Fraser FW, Fuller SJ, Smith MJ, Beyreuther K, et al. Soluble pool of Abeta amyloid as a determinant of severity of neurodegeneration in Alzheimer's disease. Ann Neurol 1999;46(6):860–6.
44. Harada R, Okamura N, Furumoto S, Tago T, Maruyama M, Higuchi M, et al. Comparison of the binding characteristics of [18F]THK-523 and other amyloid imaging tracers to Alzheimer's disease pathology. Eur J Nucl Med Mol Imaging 2013;40(1):125–32. doi:10.1007/s00259-012-2261-2.

Authors' contributions

Dr. Villemagne had full access to all the data in the study and takes responsibility for the integrity of the data and the accuracy of the data analysis

Drs. Villemagne, Furumoto, Fodero-Tavoletti, Kudo, Rowe and Okamura participated in the design, acquisition, analysis and interpretation of the data and writing of this manuscript.

Study concept and design: Villemagne, Okamura, Kudo, Rowe

Acquisition of data: Villemagne, Rowe, Fodero-Tavoletti, Pejoska, Yates, Piguet, Mulligan

Analysis and interpretation of data: Villemagne, Doré, Rowe, Okamura

Drafting of the manuscript: Villemagne, Okamura

Critical revision of the manuscript for important intellectual content: Villemagne, Furumoto, Rowe, Harada, Fodero-Tavoletti, Piguet, Hodges, Yanai, Masters, Kudo, Okamura

Statistical analysis: Villemagne, Okamura

Study supervision: Villemagne, Okamura

Curr Neurol Neurosci Rep (2014) 14:500
DOI 10.1007/s11910-014-0500-6

NEUROIMAGING (DJ BROOKS, SECTION EDITOR)

Tau PET Imaging in Alzheimer's Disease

Nobuyuki Okamura · Ryuichi Harada · Shozo Furumoto · Hiroyuki Arai · Kazuhiko Yanai · Yukitsuka Kudo

Published online: 21 September 2014
© Springer Science+Business Media New York 2014

Abstract In several neurodegenerative diseases that are collectively called tauopathies, progressive accumulation of tau in the brain is closely associated with neurodegeneration and cognitive impairment. Noninvasive detection of tau protein deposits in the brain would be useful to diagnose tauopathies as well as to track and predict disease progression. Recently, several tau PET tracers including T807, THK-5117, and PBB3 have been developed and succeeded in imaging neurofibrillary pathology in vivo. For use of tau PET as a biomarker of tau pathology in Alzheimer's disease, PET tracers should have high affinity to PHF-tau and high selectivity for tau over amyloid-β and other protein deposits. PET tau imaging enables the longitudinal assessment of the spatial pattern of tau deposition and its relation to amyloid-β pathology and neurodegeneration. This technology could also be applied to the pharmacological assessment of anti-tau therapy, thereby allowing preventive interventions.

Keywords Positron emission tomography · Amyloid · Tau · Neurofibrillary tangles · Dementia · Early diagnosis · Biomarker

This article is part of the Topical Collection on *Neuroimaging*

N. Okamura · K. Yanai
Department of Pharmacology, Tohoku University School of Medicine, 2-1, Seiryo-machi, Aoba-ku, Sendai 9808575, Japan

K. Yanai
e-mail: yanai@med.tohoku.ac.jp

N. Okamura (✉) · R. Harada · Y. Kudo
Division of Neuro-imaging, Institute of Development, Aging and Cancer, Tohoku University, 4-1, Seiryo-machi, Aoba-ku, Sendai 9808575, Japan
e-mail: nookamura@med.tohoku.ac.jp

R. Harada
e-mail: dragon1@med.tohoku.ac.jp

Y. Kudo
e-mail: kudoyk3y7k3@med.tohoku.ac.jp

S. Furumoto
Frontier Research Institute for Interdisciplinary Science, Tohoku University, 6-3, Aoba, Aramaki, Aoba-ku, Sendai 9808578, Japan
e-mail: furumoto@cyric.tohoku.ac.jp

S. Furumoto
Cyclotron and Radioisotope Center, Tohoku University, 6-3, Aoba, Aramaki, Aoba-ku, Sendai 9808578, Japan

H. Arai
Department of Geriatrics and Gerontology, Institute of Development, Aging and Cancer, Tohoku University, 4-1, Seiryo-machi, Aoba-ku, Sendai 9808575, Japan
e-mail: harai@idac.tohoku.ac.jp

Introduction

Senile plaques (SPs) and neurofibrillary tangles (NFTs) are neuropathological hallmarks of Alzheimer's disease (AD). These protein deposits, SP and NFT, are composed of amyloid-β (Aβ) protein and hyperphosphorylated tau protein, respectively. A definitive diagnosis of AD can be established by the post mortem examination of the human brain. The amyloid cascade hypothesis, which proposes that abnormal production and accumulation of Aβ is the cause of AD, has been widely accepted as the concept of AD pathogenesis [1]. Preclinical amyloid pathology that has been observed in recent amyloid PET studies is considered as a high risk for future cognitive decline [2]. Many candidates for anti-amyloid drugs have been developed to reduce the amount of Aβ [3]. However, repeated failures of clinical trials for these drugs have increased, and shifted, our interest in using tau as another target for novel drug development [4, 5].

Hyperphosphorylation of the tau protein in AD forms insoluble fibers named paired helical filaments (PHFs) [6, 7]. PHFs accumulate in the neuronal cytoplasm and form NFTs [8, 9]. Initially, NFTs occur in the transentorhinal area, followed by the involvement of the entorhinal cortex and hippocampus, progressing to the temporal cortex and the other cortical areas [10, 11]. Postmortem studies have shown that the NFT, but not the SP, load correlates with the severity of dementia and neurodegeneration [12, 13], suggesting a more direct effect of tau aggregation on neurodegeneration than Aβ.

To facilitate the development of anti-tau drugs, it is important to measure the pathologic time course of NFT formation in the human brain. Recent developments allow us to visualize NFTs in the human brain using positron emission tomography (PET) by measuring the distribution of intravenously administered radiotracers that selectively bind to NFTs. Also, PET imaging is potentially useful for monitoring treatment outcomes and selecting patients for anti-dementia therapy [14].

Requirement for Tau PET Tracers

For using PET as a biomarker of tau pathology, the imaging measures should be quantitative, reproducible, and directly linked to the presence of tau deposits in the brain. Recently, several PET tracers have been developed for imaging tau pathology in the human brain [15–17]. Most of these tracers bind to the β-pleated sheet structure of tau protein fibrils in the same way as amyloid PET ligands. Therefore, these tracers are considered to be insensitive to tau oligomers. The ideal characteristics of tau-selective PET tracers are listed in Table 1. For successful imaging of NFTs in the AD brain, the tracer should have high binding affinity to PHF-tau. The binding affinity of tracers can be quantitatively evaluated by protein-ligand binding assay using synthetic tau fibrils or human brain homogenates. The assay using synthetic protein fibrils is widely used for the screening of protein-binding ligands. However, the measured value from synthetic fibrils should be interpreted cautiously because these fibrils do not completely imitate the conformation of native tau deposits.

The assay using human brain samples is a more reliable method for the assessment of protein-ligand interaction than using synthetic fibrils. This method has been used for the assessment of amyloid-binding PET ligands [18, 19]. Most amyloid PET ligands exhibit high binding affinities to AD brain homogenates (Kd or Ki<20 nM) [20–23]. Tau PET ligands are also required to exhibit similar affinity to AD brain samples in region where NFTs are frequent (e.g. entorhinal cortex, hippocampus, and temporal cortex). In AD neocortex, the concentrations of tau are ~5–20 times lower than those of Aβ [16]. Therefore, tracers should be highly selective for tau over Aβ. Simulation studies estimate that a 20-50-fold selectivity for PHF-tau over Aβ will be required for selective imaging of PHF-tau in vivo [24]. The most reliable method for the assessment of radioligand binding selectivity is autoradiography of human brain sections, because the binding of ligands to tau fibrils can be directly assessed at a low nanomolar ligand concentration, which is achieved in the brain tissue during a PET scan. If the ligand has autofluorescence, ligand binding can also be evaluated microscopically. However, this method generally requires micromolar concentration of ligands, which is far higher than radiotracer concentrations in the brain. Lipophilic fluoro-amyloid β-sheet binding PET tracers tend to accumulate in the white matter as well as Alzheimer cortex, possibly because myelin contains β-sheet structures. Such non-specific white matter tracer binding needs to be kept minimal when developing PET ligands for tau.

In addition to these binding properties, radiotracers should have high blood–brain barrier (BBB) permeability. Most successful amyloid-PET tracers show an initial brain uptake above 4 % of the injected dose (%ID) at 2 min after intravenous injection in mice [23, 25, 26]. Lipophilicity is one of the most important determinants of BBB permeability. Ideally, a radiotracer should exhibit LogP values between 0.9 and 2.5 [27]. In addition, radiotracers should be cleared rapidly from background and non-target areas. Slower clearance of radiotracers prolongs the time for them to reach a secular equilibrium in a PET study. The brain 2-to-30 min ratio in normal mice is a good index of the clearance of radiotracer from non-target areas. The

Table 1 Ideal characteristics of tau PET tracers

Characteristics	Requirements
High binding affinity for PHF-tau	Kd or Ki<20 nM for tau-rich brain samples
High binding selectivity for PHF-tau	>20 fold selectivity for PHF-tau over Aβ
High blood–brain barrier permeability	>4 % ID/g at 2 min post injection in normal mice
Rapid clearance from normal brain tissue	2 min-to-30 min brain uptake ratio in mice>10
Moderate lipophilicity	LogP=1–3
Low non-specific binding	Low or no binding to subcortical white matter
Low metabolism	Metabolites should not enter into the brain

successful amyloid PET tracer [^{11}C]PiB shows high 2-to-30 min ratio (>10), reflecting a fast clearance from non-target regions [23]. An ideal radiotracer should readily enter the brain and selectively bind to its target in the absence of radiolabeled metabolites. Thus, the radiolabeled metabolites should not penetrate BBB. ^{18}F-labeled tracers are more clinically useful than ^{11}C-labeled tracers as the longer lived ^{18}F isotope allows time for tracer delivery to many PET centers [28]. Three ^{18}F-labeled amyloid PET tracers, including [^{18}F]florbetapir (Amyvid™), [^{18}F]flutemetamol (Vizamyl™), [^{18}F]florbetaben (Neuraceq™), have become commercially available in EU and US. However, in some ^{18}F-labeled ligands, defluorination can cause bone accumulation of ^{18}F, which might interfere with visual assessment of tracer distribution in the brain.

Tau PET in Clinical Studies

FDDNP

The first successful PET tau imaging in humans was accomplished by using [^{18}F]FDDNP [29]. In the autoradiography of the AD brain sections raised [^{18}F]FDDNP binding was detected in the hippocampus where a high density of NFTs were observed by immunohistochemistry [30]. Patients with AD and 50 % of mild cognitive impairment (MCI) cases showed higher [^{18}F]FDDNP retention than healthy control subjects [31]. A direct comparison between FDDNP and PiB in the same AD patients found negligible PiB but strong FDDNP binding in the medial temporal cortex, compatible with FDDNP binding to NFTs [32]. However, FDDNP uptake was also increased in amyloid rich cortical association areas in AD. Intriguingly, recent [^{18}F]FDDNP PET study demonstrated an elevated FDDNP uptake in the subcortical brain areas and amygdala of football players suspected of chronic traumatic encephalopathy (CTE) [33], suggesting the potential utility of PET imaging for monitoring pathological tau deposits after traumatic brain injury [34]. Furthermore, [^{18}F]FDDNP is reported to be sensitive in imaging the regional localization of tau deposits in progressive supranuclear palsy (PSP) [35]. However, there are some limitations for use of this tracer as a biomarker of tau, because this tracer binds non-selectively to both SPs and NFTs and is less sensitive to tau deposits than more recently developed radiotracers shown below.

PBB3

[^{11}C]PBB3 is a PET tracer that is reported to allow in vivo detection of tau deposits in AD as well as in non-AD tauopathies, including PSP and corticobasal degeneration (CBD) [36•]. In clinical PET studies, this tracer can be produced with sufficient radioactivity and high quality [37] and it clearly differentiated AD brains from healthy control brains [36•]. [^{11}C]PBB3 retention in the hippocampus of AD patients confirms the binding ability of this tracer to NFTs. In addition, this study reported significant [^{11}C]PBB3 binding to tau deposits in the basal ganglia of a CBD case. Ongoing multicenter PET studies of [^{11}C]PBB3 will validate the clinical usefulness of this tracer in various types of tauopathies.

T807 and T808

[^{18}F]T807 and [^{18}F]T808 have been developed as tau-selective PET tracers [38•, 39, 40]. In vitro autoradiography studies showed that both radiotracers exhibit strong and selective binding to PHF-tau with nanomolar affinity on AD brain sections with little binding to amyloid plaques. The first-in-man PET study successfully demonstrated [^{18}F]T807 retention in the frequent areas of PHF-tau in the AD brain [38•]. In addition, [^{18}F]T807 retention was associated with increased disease severity. There was much more elevated and extensive [^{18}F]T807 retention in severe AD case than in MCI and mild AD cases. Unlike most ^{18}F-labeled amyloid PET tracers, [^{18}F]T807 shows very low non-specific binding of the tracer to the white matter, which may improve the grey-to-white matter contrast in the brain. The first-in-man PET studies of [^{18}F]T808 were performed in 11 subjects [39]. This tracer showed more rapid tracer distribution throughout the brain and more rapid clearance from normal brain tissue than [^{18}F]T807. Most AD cases showed elevated [^{18}F]T808 retention in the frequent areas of PHF-tau. However, substantial defluorination was observed in some cases.

THK-523, THK-5105 and THK-5117

Novel quinoline derivatives were initially identified as candidates for tau PET tracer by the screening of over 2,000 small molecules [41]. In vitro autoradiography studies using three ^{18}F-labeled derivatives ([^{18}F]THK-523, [^{18}F]THK-5105 and [^{18}F]THK-5117) demonstrated the high binding selectivity of these tracers to tau over Aβ on AD brain sections [42–44]. While [^{18}F]THK-523 PET failed to clearly visualize tau deposits in the human brain in vivo [45],. [^{18}F]THK-5105 PET successfully demonstrated radiotracer retention in sites susceptible to tau deposition in the AD brain [46••]. Recent [^{18}F]THK-5117 PET studies demonstrated higher signal-to-background ratio and better pharmacokinetics of this tracer than [^{18}F]THK-5105 [17]. [^{18}F]THK-5117 PET images in mild, moderate and severe AD patients are shown in Fig. 1. These tracer retentions were associated with clinical severity of dementia and brain atrophy [46••], which is consistent with the observation of postmortem brain analysis showing the association of tau pathology with dementia severity and neuronal loss.

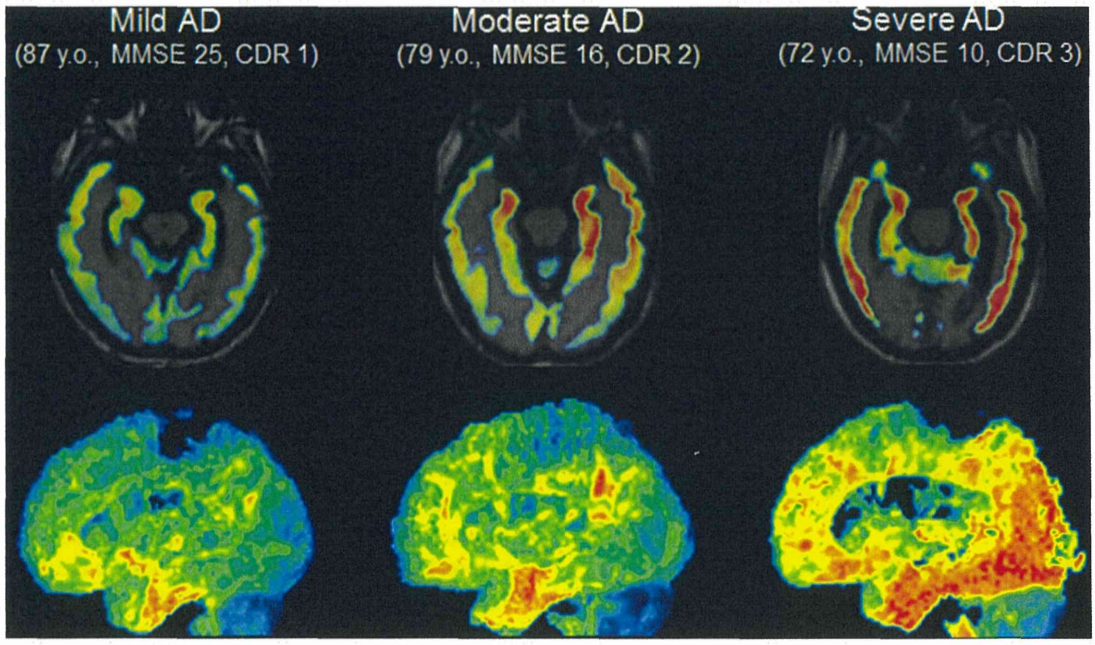

Fig. 1 [^{18}F]THK-5117 PET images in mild, moderate and severe AD patients. In mild AD case, specific [^{18}F]THK-5117 binding is confined to the medial, anterior and inferior temporal cortex. Moderate AD case shows additional [^{18}F]THK-5117 retention in association areas. Severe AD case shows more extensive and higher [^{18}F]THK-5117 retention in the neocortex

Potential role of Tau PET Imaging

PET enables us to study the interaction of Aβ and tau and their influences on neurodegenerative processes in the human brain. Tau PET has many target diseases including AD, frontotemporal dementia, PSP, CBD and CTE [15, 47] (Table 2). Recent PET studies described above have shown the potential utility of tau imaging for the diagnosis of non-AD tauopathies. One good example is CTE. CTE is known as a progressive tauopathy associated with repetitive traumatic brain injury [34, 48]. The pathology of CTE is characterized by the accumulation of phosphorylated tau protein in neurons and astrocytes. The morphological appearance of tau deposits in CTE is similar to that found in AD, however the spatial pattern of tau deposition is different from AD [49]. Therefore, tau imaging might distinguish the pathology related with CTE from AD by the pattern of tracer distribution. However, tau PET might not be able to visualize all kinds of tau deposits in vivo, because the conformation of protein fibrils is different in each disease and in each pathological deposit. Another

Table 2 Comparison of amyloid and tau PET imaging

	Amyloid PET	Tau PET
Radiotracer	[^{11}C]PiB [^{11}C]BF227 [^{18}F]Flutemetamol [^{18}F]Florbetapir [^{18}F]Florbetaben [^{18}F]NAV4694	[^{11}C]PBB3 [^{18}F]T807 [^{18}F]T808 [^{18}F]THK-5105 [^{18}F]THK-5117
Target diseases	Alzheimer's disease	Alzheimer's disease Frontotemporal dementia Progressive supranuclear palsy Corticobasal degeneration Chronic traumatic encephalopathy Senile dementia of the neurofibrillary tangle type Argyrophilic grain disease
Frequent areas of tracer uptake in Alzheimer's disease	Neocortex	Medial and lateral temporal cortex
Neocortical tracer retention in an asymptomatic state	Frequent	Rare
Association with clinical severity of dementia	No or little	High
Association with neurodegeneration	No or little	High

concern is whether the density of tau deposits in the brain is sufficient for in vivo detection or not.

Tau pathology is strongly associated with age and is frequently observed in late-onset dementias. Some of these cases are pathologically diagnosed as senile dementia of the neurofibrillary tangle type [50] or argyrophilic grain disease [51]. Tau PET might be useful for antemortem diagnosis of these diseases which differ from AD as amyloid PET gives negative results in these tauopathies [52]. Recent studies have shown that a population labelled suspected non-AD pathophysiology (SNAP) exists who have abnormal neurodegeneration biomarkers (atrophy, glucose hypometabolism) but absent brain amyloid pathology [53]. The pathological condition of these populations might be partially explained by the existence of tau pathology.

The distribution of amyloid PET tracers is diffuse and widespread in the neocortex. Even where widespread Aβ deposits exist in cognitively normal subjects, cortical tau pathology can be unremarkable [54] indicating that amyloid pathology is upstream of tau pathology in the neocortex [55, 56]. Presymptomatic Aβ pathology is recognized as a high risk factor for future progression to dementia [54]. However, amyloid PET studies have shown little association of brain amyloid load with clinical severity of dementia in AD patients, suggesting that the presence of Aβ plaques alone is not sufficient to produce cognitive impairment [57, 58]. In contrast, tau pathology in AD starts within a very limited area (medial temporal cortex) of the brain, and then gradually spreads to the neocortex as the clinical symptom of dementia progress. Pattern of tau pathology are strongly associated with neurodegeneration, reflected by brain atrophy [59]. In postmortem studies, NFTs in the hippocampal as well as temporal cortex were observed in MCI cases and in cases having very early symptomatic signs of dementia [11, 60]. Recent PET studies have successfully detected tau pathology in brain areas of mild AD cases [38•, 40, 45]. Therefore, the amount and extent of tau pathology could be a good marker of the severity and prognosis of preclinical AD and MCI. Tau deposits in the medial temporal cortex have been considered to be age-related, and are independent of AD disease process. However, the progression of tau pathology might be accelerated, inducing neurodegeneration and cognitive decline, once Aβ deposits start to accumulate in the neocortex [61–63]. The synergistic effect of these two protein deposits and their influences on neurodegenerative process should be clarified in the future by carrying out longitudinal analysis of tau and amyloid PET data.

Conclusions

Several PET tracers that have been developed for imaging PHF-tau have shown promising results in humans. These tracers are reported to be selective for PHF-tau in vitro. Additional studies are required to evaluate their reliability and quantitative performance, and to validate the in vivo binding selectivity of these tracers to tau pathology. PET tau imaging would be useful for early detection of disease-related pathology, for pharmacological evaluation of drug efficacy and for understanding the pathophysiology in AD and non-AD tauopathies. Longitudinal PET studies will clarify the interaction of tau and Aβ, and their influences on neurodegenerative process in the human brain.

Compliance with Ethics Guidelines

Conflict of Interest Ryuichi Harada, Hiroyuki Arai, and Kazuhiko Yanai declare that they have no conflict of interest.

Nobuyuki Okamura, Shozo Furumoto, and Yukitsuka Kudo were funded by a grant to study tau PET imaging from GE Healthcare, the SEI (Sumitomo Electric Industries, Ltd.) Group, CSR Foundation, Health and Labor Sciences Research Grants from the Ministry of Health, Labor, and Welfare of Japan, and Grant-in-Aid for Exploratory Research (25670524) of the Ministry of Education, Culture, Sports, Science and Technology (MEXT), Japan.

Human and Animal Rights and Informed Consent This article does not contain any studies with human or animal subjects performed by any of the authors.

References

Papers of particular interest, published recently, have been highlighted as:
- • Of importance
- •• Of major importance

1. Hardy J, Selkoe DJ. The amyloid hypothesis of Alzheimer's disease: progress and problems on the road to therapeutics. Science. 2002;297:353–6.
2. Sperling RA, Aisen PS, Beckett LA, Bennett DA, Craft S, Fagan AM, et al. Toward defining the preclinical stages of Alzheimer's disease: recommendations from the National Institute on Aging-Alzheimer's association workgroups on diagnostic guidelines for Alzheimer's disease. Alzheimers Dement. 2011;7:280–92.
3. Citron M. Alzheimer's disease: strategies for disease modification. Nat Rev Drug Discov. 2010;9:387–98.
4. Giacobini E, Gold G. Alzheimer disease therapy–moving from amyloid-beta to tau. Nat Rev Neurol. 2013;9:677–86.
5. Ballatore C, Lee VM, Trojanowski JQ. Tau-mediated neurodegeneration in Alzheimer's disease and related disorders. Nat Rev Neurosci. 2007;8:663–72.
6. Grundke-Iqbal I, Iqbal K, Tung YC, Quinlan M, Wisniewski HM, Binder LI. Abnormal phosphorylation of the microtubule-associated protein tau (tau) in Alzheimer cytoskeletal pathology. Proc Natl Acad Sci U S A. 1986;83:4913–7.
7. Grundke-Iqbal I, Iqbal K, Quinlan M, Tung YC, Zaidi MS, Wisniewski HM. Microtubule-associated protein tau. A component of Alzheimer paired helical filaments. J Biol Chem. 1986;261:6084–9.
8. Price JL, Davis PB, Morris JC, White DL. The distribution of tangles, plaques and related immunohistochemical markers in

healthy aging and Alzheimer's disease. Neurobiol Aging. 1991;12: 295–312.
9. Braak H, Braak E. Frequency of stages of Alzheimer-related lesions in different age categories. Neurobiol Aging. 1997;18:351–7.
10. Braak H, Braak E. Neuropathological stageing of Alzheimer-related changes. Acta Neuropathol. 1991;82:239–59.
11. Delacourte A, David JP, Sergeant N, Buee L, Wattez A, Vermersch P, et al. The biochemical pathway of neurofibrillary degeneration in aging and Alzheimer's disease. Neurology. 1999;52:1158–65.
12. Bierer LM, Hof PR, Purohit DP, Carlin L, Schmeidler J, Davis KL, et al. Neocortical neurofibrillary tangles correlate with dementia severity in Alzheimer's disease. Arch Neurol. 1995;52:81–8.
13. Arriagada PV, Growdon JH, Hedley-Whyte ET, Hyman BT. Neurofibrillary tangles but not senile plaques parallel duration and severity of Alzheimer's disease. Neurology. 1992;42:631–9.
14. Nordberg A, Rinne JO, Kadir A, Langstrom B. The use of PET in Alzheimer disease. Nat Rev Neurol. 2010;6:78–87.
15. Villemagne VL, Okamura N. In vivo tau imaging: obstacles and progress. Alzheimers Dement. 2014;10:S254–64.
16. Villemagne VL, Furumoto S, Fodero-Tavoletti MT, Harada R, Mulligan RS, Kudo Y, et al. The challenges of tau imaging. Futur Neurol. 2012;7:409–21.
17. Shah M, Catafau AM. Molecular Imaging Insights into neurodegeneration: focus on Tau PET Radiotracers. J Nucl Med. 2014;55: 871–4.
18. Fodero-Tavoletti MT, Smith DP, McLean CA, Adlard PA, Barnham KJ, Foster LE, et al. In vitro characterization of Pittsburgh compound-B binding to Lewy bodies. J Neurosci. 2007;27: 10365–71.
19. Fodero-Tavoletti MT, Mulligan RS, Okamura N, Furumoto S, Rowe CC, Kudo Y, et al. In vitro characterisation of BF227 binding to alpha-synuclein/Lewy bodies. Eur J Pharmacol. 2009;617:54–8.
20. Ni R, Gillberg PG, Bergfors A, Marutle A, Nordberg A. Amyloid tracers detect multiple binding sites in Alzheimer's disease brain tissue. Brain. 2013;136:2217–27.
21. Choi SR, Golding G, Zhuang Z, Zhang W, Lim N, Hefti F, et al. Preclinical properties of 18 F-AV-45: a PET agent for Abeta plaques in the brain. J Nucl Med. 2009;50:1887–94.
22. Klunk WE, Wang Y, Huang GF, Debnath ML, Holt DP, Shao L, et al. The binding of 2-(4′-methylaminophenyl)benzothiazole to postmortem brain homogenates is dominated by the amyloid component. J Neurosci. 2003;23:2086–92.
23. Mathis CA, Wang Y, Holt DP, Huang GF, Debnath ML, Klunk WE. Synthesis and evaluation of 11C-labeled 6-substituted 2-arylbenzothiazoles as amyloid imaging agents. J Med Chem. 2003;46:2740–54.
24. Schafer KN, Kim S, Matzavinos A, Kuret J. Selectivity requirements for diagnostic imaging of neurofibrillary lesions in Alzheimer's disease: a simulation study. Neuroimage. 2012;60: 1724–33.
25. Choi SR, Golding G, Zhuang Z, Zhang W, Lim N, Hefti F, et al. Preclinical properties of 18 F-AV-45: a PET agent for Abeta plaques in the brain. J Neurosci. 2009;50:1887–94.
26. Snellman A, Rokka J, Lopez-Picon FR, Eskola O, Wilson I, Farrar G, et al. Pharmacokinetics of [18F]flutemetamol in wild-type rodents and its binding to beta amyloid deposits in a mouse model of Alzheimer's disease. Eur J Nucl Med Mol Imaging. 2012;39:1784–95.
27. Dischino DD, Welch MJ, Kilbourn MR, Raichle ME. Relationship between lipophilicity and brain extraction of C-11-labeled radiopharmaceuticals. J Nucl Med. 1983;24:1030–8.
28. Herholz K, Ebmeier K. Clinical amyloid imaging in Alzheimer's disease. Lancet Neurol. 2011;10:667–70.
29. Shoghi-Jadid K, Small GW, Agdeppa ED, Kepe V, Ercoli LM, Siddarth P, et al. Localization of neurofibrillary tangles and beta-amyloid plaques in the brains of living patients with Alzheimer disease. Am J Geriatr Psychiatr. 2002;10:24–35.
30. Agdeppa ED, Kepe V, Liu J, Flores-Torres S, Satyamurthy N, Petric A, et al. Binding characteristics of radiofluorinated 6-dialkylamino-2-naphthylethylidene derivatives as positron emission tomography imaging probes for beta-amyloid plaques in Alzheimer's disease. J Neurosci. 2001;21:RC189.
31. Small GW, Kepe V, Ercoli LM, Siddarth P, Bookheimer SY, Miller KJ, et al. PET of brain amyloid and tau in mild cognitive impairment. N Engl J Med. 2006;355:2652–63.
32. Shin J, Lee SY, Kim SH, Kim YB, Cho SJ. Multitracer PET imaging of amyloid plaques and neurofibrillary tangles in Alzheimer's disease. Neuroimage. 2008;43:236–44.
33. Small GW, Kepe V, Siddarth P, Ercoli LM, Merrill DA, Donoghue N, et al. PET scanning of brain tau in retired national football league players: preliminary findings. Am J Geriatr Psychiatr. 2013;21: 138–44.
34. DeKosky ST, Blennow K, Ikonomovic MD, Gandy S. Acute and chronic traumatic encephalopathies: pathogenesis and biomarkers. Nat Rev Neurol. 2013;9:192–200.
35. Kepe V, Bordelon Y, Boxer A, Huang SC, Liu J, Thiede FC, et al. PET imaging of neuropathology in tauopathies: progressive supranuclear palsy. J Alzheimers Dis. 2013;36:145–53.
36.• Maruyama M, Shimada H, Suhara T, Shinotoh H, Ji B, Maeda J, et al. Imaging of tau pathology in a tauopathy mouse model and in Alzheimer patients compared to normal controls. Neuron. 2013;79: 1094–108. *Maruyama et al. performed first-in-man PET studies of [^{11}C]PBB3 in 3 healthy controls and 3 AD patients. [^{11}C]PBB3 retention was observed in the hippocampus of AD patients, suggesting that this tracer binds to NFTs in vivo. In addition, [^{11}C]PBB3 binding to tau deposits was reported in the basal ganglia of CBD patient.*
37. Hashimoto H, Kawamura K, Igarashi N, Takei M, Fujishiro T, Aihara Y, et al. Radiosynthesis, Photoisomerization, Biodistribution, and metabolite analysis of 11C-PBB3 as a clinically useful PET probe for imaging of Tau pathology. J Nucl Med. 2014;55:1532-8.
38.• Chien DT, Bahri S, Szardenings AK, Walsh JC, Mu F, Su MY, et al. Early clinical PET imaging results with the novel PHF-tau radioligand [F-18]-T807. J Alzheimers Dis. 2013;34:457–68. *The first-in-man PET studies of [^{18}F]T807 demonstrated significant tracer retention in the frequent areas of PHF-tau in AD brain. [^{18}F]T807 retention was associated with increasing disease severity. In addition, [^{18}F]T807 shows very low non-specific binding of the tracer in the white matter.*
39. Chien DT, Szardenings AK, Bahri S, Walsh JC, Mu FR, Xia CF, et al. Early clinical PET imaging results with the Novel PHF-Tau radioligand [F18]-T808. J Alzheimers Dis. 2014;38:171–84.
40. Xia CF, Arteaga J, Chen G, Gangadharmath U, Gomez LF, Kasi D, et al. [18F]T807, a novel tau positron emission tomography imaging agent for Alzheimer's disease. Alzheimers Dement. 2013.
41. Okamura N, Suemoto T, Furumoto S, Suzuki M, Shimadzu H, Akatsu H, et al. Quinoline and benzimidazole derivatives: candidate probes for in vivo imaging of tau pathology in Alzheimer's disease. J Neurosci. 2005;25:10857–62.
42. Fodero-Tavoletti MT, Okamura N, Furumoto S, Mulligan RS, Connor AR, McLean CA, et al. ^{18} F-THK523: a novel in vivo tau imaging ligand for Alzheimer's disease. Brain. 2011;134:1089–100.
43. Harada R, Okamura N, Furumoto S, Tago T, Maruyama M, Higuchi M, et al. Comparison of the binding characteristics of [^{18} F]THK-523 and other amyloid imaging tracers to Alzheimer's disease pathology. Eur J Nucl Med Mol Imaging. 2013;40:125–32.
44. Okamura N, Furumoto S, Harada R, Tago T, Yoshikawa T, Fodero-Tavoletti M, et al. Novel ^{18} F-labeled arylquinoline derivatives for noninvasive imaging of tau pathology in Alzheimer disease. J Nucl Med. 2013;54:1420–7.
45. Villemagne VL, Furumoto S, Fodero-Tavoletti MT, Mulligan RS, Hodges J, Harada R, et al. In vivo evaluation of a novel tau imaging tracer for Alzheimer's disease. Eur J Nucl Med Mol Imaging. 2014;41:816-26.

46.•• Okamura N, Furumoto S, Fodero-Tavoletti MT, Mulligan RS, Harada R, Yates P, et al. Non-invasive assessment of Alzheimer's disease neurofibrillary pathology using ^{18}F-THK5105 PET. Brain. 2014;137:1762–71. *The first-in man studies of [^{18}F]THK-5105 demonstrated tracer retention in the frequent areas of PHF-tau in AD brain. Tracer retention was associated with clinical severity of dementia and brain atrophy, which is consistent with the observation of postmortem studies.*

47. Fodero-Tavoletti MT, Furumoto S, Taylor L, McLean CA, Mulligan RS, Birchall I, et al. Assessing THK523 selectivity for tau deposits in Alzheimer's disease and non Alzheimer's disease tauopathies. Alzheimers Res Ther. 2014;6:11.

48. Stein TD, Alvarez VE, McKee AC. Chronic traumatic encephalopathy: a spectrum of neuropathological changes following repetitive brain trauma in athletes and military personnel. Alzheimers Res Ther. 2014;6:4.

49. McKee AC, Stern RA, Nowinski CJ, Stein TD, Alvarez VE, Daneshvar DH, et al. The spectrum of disease in chronic traumatic encephalopathy. Brain. 2013;136:43–64.

50. Yamada M, Itoh Y, Sodeyama N, Suematsu N, Otomo E, Matsushita M, et al. Senile dementia of the neurofibrillary tangle type: a comparison with Alzheimer's disease. Dement Geriatr Cogn Disord. 2001;12:117–26.

51. Saito Y, Ruberu NN, Sawabe M, Arai T, Tanaka N, Kakuta Y, et al. Staging of argyrophilic grains: an age-associated tauopathy. J Neuropathol Exp Neurol. 2004;63:911–8.

52. Takeuchi J, Shimada H, Ataka S, Kawabe J, Mori H, Mizuno K, et al. Clinical features of Pittsburgh compound-B-negative dementia. Dement Geriatr Cogn Disord. 2012;34:112–20.

53. Jack Jr CR, Knopman DS, Weigand SD, Wiste HJ, Vemuri P, Lowe V, et al. An operational approach to National Institute on Aging-Alzheimer's association criteria for preclinical Alzheimer disease. Ann Neurol. 2012;71:765–75.

54. Morris JC, Price JL. Pathologic correlates of nondemented aging, mild cognitive impairment, and early-stage Alzheimer's disease. J Mol Neurosci. 2001;17:101–18.

55. Jack Jr CR, Knopman DS, Jagust WJ, Petersen RC, Weiner MW, Aisen PS, et al. Tracking pathophysiological processes in Alzheimer's disease: an updated hypothetical model of dynamic biomarkers. Lancet Neurol. 2013;12:207–16.

56. Perrin RJ, Fagan AM, Holtzman DM. Multimodal techniques for diagnosis and prognosis of Alzheimer's disease. Nature. 2009;461:916–22.

57. Rabinovici GD, Jagust WJ. Amyloid imaging in aging and dementia: testing the amyloid hypothesis in vivo. Behav Neurol. 2009;21:117–28.

58. Jack Jr CR, Lowe VJ, Weigand SD, Wiste HJ, Senjem ML, Knopman DS, et al. Serial PIB and MRI in normal, mild cognitive impairment and Alzheimer's disease: implications for sequence of pathological events in Alzheimer's disease. Brain. 2009;132:1355–65.

59. Whitwell JL, Josephs KA, Murray ME, Kantarci K, Przybelski SA, Weigand SD, et al. MRI correlates of neurofibrillary tangle pathology at autopsy: a voxel-based morphometry study. Neurology. 2008;71:743–9.

60. Hof PR, Bierer LM, Perl DP, Delacourte A, Buee L, Bouras C, et al. Evidence for early vulnerability of the medial and inferior aspects of the temporal lobe in an 82-year-old patient with preclinical signs of dementia. Regional and laminar distribution of neurofibrillary tangles and senile plaques. Arch Neurol. 1992;49:946–53.

61. Csernansky JG, Hamstra J, Wang L, McKeel D, Price JL, Gado M, et al. Correlations between antemortem hippocampal volume and postmortem neuropathology in AD subjects. Alzheimer Dis Assoc Disord. 2004;18:190–5.

62. Csernansky JG, Wang L, Swank J, Miller JP, Gado M, McKeel D, et al. Preclinical detection of Alzheimer's disease: hippocampal shape and volume predict dementia onset in the elderly. Neuroimage. 2005;25:783–92.

63. Delacourte A, Sergeant N, Wattez A, Maurage CA, Lebert F, Pasquier F, et al. Tau aggregation in the hippocampal formation: an ageing or a pathological process? Exp Gerontol. 2002;37:1291–6.

Fodero-Tavoletti et al. Alzheimer's Research & Therapy 2014, 6:11
http://alzres.com/content/6/1/11

alzheimer's research&therapy

RESEARCH Open Access

Assessing THK523 selectivity for tau deposits in Alzheimer's disease and non–Alzheimer's disease tauopathies

Michelle T Fodero-Tavoletti[1,2*], Shozo Furumoto[3], Leanne Taylor[1], Catriona A McLean[4], Rachel S Mulligan[2], Ian Birchall[1], Ryuichi Harada[3], Colin L Masters[1], Kazuhiko Yanai[3], Yukitsuka Kudo[5], Christopher C Rowe[2], Nobuyuki Okamura[3] and Victor L Villemagne[1,2]

Abstract

Introduction: The introduction of tau imaging agents such as ^{18}F-THK523 offers new hope for the *in vivo* assessment of tau deposition in tauopathies such as Alzheimer's disease (AD), where preliminary ^{18}F-THK523-PET studies have demonstrated significantly higher cortical retention of ^{18}F-THK523 in AD compared to age-matched healthy individuals. In addition to AD, tau imaging with PET may also be of value in assessing non-AD tauopathies, such as corticobasal degeneration (CBD), progressive supranuclear palsy (PSP) and Pick's disease (PiD).

Methods: To further investigate the ability of THK523 to recognize tau lesions, we undertook immunohistochemical and fluorescence studies in serial brain sections taken from individuals with AD ($n = 3$), CBD ($n = 2$), PSP ($n = 1$), PiD ($n = 2$) and Parkinson's disease (PD; $n = 2$). In addition to the neuropathological analysis, one PSP patient had undergone a ^{18}F-THK523 PET scan 5 months before death.

Results: Although THK523 labelled tau-containing lesions such as neurofibrillary tangles and neuropil threads in the hippocampus and frontal regions of AD brains, it failed to label tau-containing lesions in non-AD tauopathies. Furthermore, though THK523 faintly labelled dense-cored amyloid-β plaques in the AD frontal cortex, it failed to label α-synuclein-containing Lewy bodies in PD brain sections.

Conclusion: The results of this study suggest that ^{18}F-THK523 selectively binds to paired helical filament tau in AD brains but does not bind to tau lesions in non-AD tauopathies, or to α-synuclein in PD brains.

Introduction

Alzheimer's disease (AD) is the most common form of dementia (50% to 70% of dementia cases) [1]. At present, there is no cure for the disease. Age is the greatest risk factor. Despite the existence of distinctive clinical diagnostic criteria, the differential diagnosis of AD and other neurodegenerative disorders is sometimes challenging because of substantial overlap in clinical presentations, especially at the early stages of the disease [2]. Consequently, making the definitive diagnosis of neurodegenerative diseases is still reliant upon postmortem examination of the brain.

AD is pathologically characterised by the presence of (1) extracellular neuritic plaques composed of aggregated β-amyloid (Aβ) and (2) intracellular neurofibrillary tangles (NFTs) composed of the aggregated tau protein [3,4]. Tau aggregates are a pathological trait of not only AD but also other neurodegenerative conditions, such as corticobasal degeneration (CBD) and progressive supranuclear palsy (PSP), as well as some variants of frontotemporal lobar degeneration (FTLD-tau) [5], such as Pick's disease (PiD). Whilst the underlying mechanism leading to tau accumulation remains unclear, it is thought to be related to several pathogenic events resulting in hyperphosphorylation, misfolding and aggregation of tau. Tau aggregation in this wide spectrum of tauopathies presents

* Correspondence: m.fodero@unimelb.edu.au
[1]The Florey Institute of Neuroscience and Mental Health, 30 Royal Parade, Parkville, 3052 Melbourne, Victoria, Australia
[2]Department of Nuclear Medicine & Centre for PET, Austin Health, 145 Studley Road, Heidelberg, 3084 Melbourne, Victoria, Australia
Full list of author information is available at the end of the article

BioMed Central

© 2014 Fodero-Tavoletti et al.; licensee BioMed Central Ltd. This is an Open Access article distributed under the terms of the Creative Commons Attribution License (http://creativecommons.org/licenses/by/2.0), which permits unrestricted use, distribution, and reproduction in any medium, provided the original work is properly credited.

with different morphologies (for example, NFTs in AD, astrocytes in CBD, globose tangles and thorny and tufted astrocytes in PSP and Pick bodies in PiD [6-9]) and ultrastructural conformations (for example, paired helical filaments in AD, straight filaments in PSP and twisted ribbons and random coils in PiD [6,10,11]), which are probably attributable to the combinations of the different tau isoforms and a wide variety of posttranslation modifications [6,12]. Additionally, the spatial distribution of the tau aggregates in these tauopathies differ from each other, with NFTs in AD being prevalent in the mesial temporal cortex and cortical grey-matter (GM) areas. Tau aggregates are also found in the frontal and striatal brain regions in CBD; in the brainstem, cerebellar white matter and basal ganglia in PSP; and in the frontal and temporal neocortex in PiD [13-17]. The diverse distribution of these tau aggregates in the brain can potentially be useful in the differential diagnosis of these tauopathies, assuming the same tau imaging agent binds with similar affinity to the whole spectrum of tau aggregates. Alternatively, the differential diagnosis might require the development of selective tau radiotracers for each specific conformation of tau aggregates.

In recent years, a great deal of interest has been placed on identifying the ideal diagnostic tool for neurodegenerative diseases. Despite the quantitative assessment of Aβ, tau and phospho-tau in cerebrospinal fluid (CSF) [18], lumbar puncture is still considered an invasive procedure for the widespread screening of the 'at-risk' population. Additionally, CSF measurements do not provide information on regional brain deposition of Aβ or tau, which may have clear correlates with cognition or regional brain atrophy and might not be able to provide important information regarding the therapeutic outcomes or response to current drugs aimed at modulating the deposition of these misfolded proteins [19-23]. Given the sometimes nonspecific nature of clinical symptoms and neuropsychological assessments, modern molecular imaging techniques have proven beneficial in the noninvasive identification of the underlying pathology of these diseases. Considerable effort has been focused on the development of novel Aβ ligands that permit detection of Aβ deposition [24]. The Aβ-specific ligands ^{18}F-AV-45 (florbetapir; (*E*)-4-(2-(6-(2-(2-(2-([^{18}F]-fluoroethoxy)ethoxy)ethoxy)pyridin-3-yl)vinyl)-N-methyl benzenamine) and Pittsburgh compound B (PiB) [25] are the best characterized and have proven to be suitable positron emission tomography (PET) biomarkers for the *in vivo* quantitation of cerebral Aβ burden. They have demonstrated a robust difference in retention between AD and healthy individuals [25-27]. ^{18}F-AV-45 [27] and flutemetamol 18 (2-[3-fluoranyl-4-(methylamino)phenyl]-1,3-benzothiazol-6-ol) [28] have already been approved for clinical Aβ imaging in the United States. These two agents belong to a second generation of Aβ radiotracers labelled with ^{18}F, which, with a half-life of 110 minutes, allows a wider and more cost-effective application of Aβ imaging.

We recently reported the preclinical characterization of the selective tau radiotracer ^{18}F-THK523 [29], a quinoline derivative pioneered by Okamura and colleagues [30,31]. Preliminary clinical evaluation of ^{18}F-THK523 has demonstrated that ^{18}F-THK523 retention is significantly higher in the cortical and hippocampal GM of AD patients than in age-matched healthy individuals [32].

To discern whether ^{18}F-THK523 recognises non-AD tau aggregates in addition to NFTs, we evaluated a series of brain sections from AD and non-AD tauopathies to evaluate the binding profile of ^{18}F-THK523.

Methods

Postmortem assessment

Chemicals

All reagents were purchased from Sigma-Aldrich (St Louis, MO, USA) unless otherwise stated.

Tissue collection and characterisation

Tissues were sourced and prepared by the Victorian Brain Bank Network. The AD pathological diagnosis was made according to standard National Institute on Aging/Reagan Institute criteria [5]. Determination of age-matched control cases were subject to the above-described criteria. The pathological diagnoses of PiD, CBD and PSP were all made according to previously described methods [33,34]. Ten cases were evaluated for this study: AD ($n = 3$), CBD ($n = 1$), PiD ($n = 2$), PD ($n = 1$) and PSP ($n = 3$). One of the individuals with PSP had undergone ^{18}F-THK523 PET 5 months before death.

Immunohistochemistry and fluorescence analysis

All brain tissue was fixed in 10% neutral buffered formalin, processed, and embedded in paraffin. For immunohistochemistry, 5-μm serial sections were deparaffinized and treated with 90% formic acid for 5 minutes, and endogenous peroxidase activity was blocked with 5% hydrogen peroxide. Sections were then treated with 0.2% casein in Tris buffer before incubation with primary antibodies to α-synuclein (97/8, 1:2,000 dilution) [35], Aβ (1e8, 1:2,000 dilution; monoclonal antibody recognises Aβ(17–24)) [36] and tau (polyclonal antibody recognises C-terminal tau (amino acids 243 to 441), catalog no. 0024; Dako Denmark, Glostrup, Denmark), for 1 hour at room temperature. Serial 5-μm tissue sections were stained as follows. The first and third sections were immunolabelled with anti-97/8 antibody, anti-1e8 antibody or tau to identify Lewy bodies, Aβ plaques or tau aggregates, respectively. The second serial section was stained with unlabelled THK523 to assess whether THK523 staining colocalised with the immunodetected Lewy bodies

and/or Aβ plaques and/or tau aggregates. Detection of antibody binding was achieved using the LSAB kit (labelled streptavidin-biotin, catalog no. K0657; Dako Denmark), then sections were incubated with hydrogen peroxidase diaminobenzidine (H_2O_2-DAB; Dako Denmark) to visualise the α-synuclein-, Aβ- or tau-positive deposits. Sections were counterstained briefly (15 seconds) with Harris's haematoxylin. To detect THK523 fluorescence, quenching was first performed whereby sections were first deparaffinized and tissue autofluorescence was minimized by treatment of sections with 0.25% $KMnO_4$ phosphate-buffered saline (PBS) for 20 minutes prior to washing in PBS and incubation with 1% potassium metabisulphite/1% oxalic acid/PBS for 5 minutes. Following autofluorescence quenching, sections were blocked in 2% bovine serum albumin/PBS, pH 7.0, for 10 minutes and stained with 100 μM THK523 for 30 minutes. Sections washed in PBS were then mounted in nonfluorescent mounting medium (catalog no. S3023; Dako Denmark). Epifluorescent images were visualized on a Leica microscope (47-nm cyan fluorescent protein, fluorescence filter set 47 (EM BP 436/20, BS FT 455 and EM BP 480/40); Leica Microsystems, North Ryde, 2113 Australia). Colocalisation of the THK523 and antibody signals were assessed by overlaying images from each of the stained serial tissue sections.

Antemortem assessment

Five months before death, a seventy-nine-year-old patient diagnosed with PSP underwent an Aβ imaging PET scan with ^{18}F-florbetaben and a tau imaging scan with ^{18}F-THK523. Approval of the study was granted by the Austin Health Human Research Ethics Committee, and written informed consent was obtained from all participants and caregivers before the study. The patient was recruited, reviewed and diagnosed on the basis of clinical and neuropsychological assessment by consensus of a neurologist and a neuropsychologist.

As part of the imaging protocol, we performed magnetic resonance imaging (MRI) using a three-dimensional magnetization-prepared rapid acquisition gradient echo sequence and T2-weighted fast spin echo and fluid-attenuated inversion recovery sequences. Both ^{18}F-florbetaben and ^{18}F-THK523 were synthesized at the Centre for PET, Austin Health, as previously described [37-39]. PET scans were acquired using a Philips Allegro PET scanner (Philips Healthcare, North Ryde, Australia) at the Austin Health Centre. A transmission scan using a rotating Cs-137 source was taken for attenuation correction immediately prior to obtaining the emission scan. A 60-minute list-mode emission acquisition, followed by a 90- to 120-minute acquisition using 10-minute frames, was performed in three-dimensional mode after injection of 300 MBq of ^{18}F-florbetaben. A 90-minute list-mode emission image acquisition was performed in three-dimensional mode after injection of 200 MBq of ^{18}F-THK523. Images were reconstructed using a three-dimensional row action maximum likelihood algorithm.

PET images were processed using a previously described semiautomatic region of interest (ROI) method [40]. Briefly, coregistration of the patient's MRI scans with the PET images was performed with Statistical Parametric Mapping 8 (SPM8) software [41]. A narrow cortical ROI template was placed on the coregistered MRI scanner by an operator (VLV) who was blinded to the participant's clinical status, then it was transferred to the coregistered PET images. The ROI template covered cortical and subcortical GM structures as well as the midbrain and pons. Subcortical white-matter ROIs were placed at the centrum semiovale, and the cerebellar regions were placed over the cerebellar cortex, taking care to avoid white matter. Standardised uptake values (SUVs), defined as the decay-corrected brain radioactivity concentration normalized for injected dose and body weight, were calculated for all regions. In order to avoid arterial blood sampling, a simplified approach was applied using the cerebellar cortex as the reference region. SUVs were used to derive SUV ratios (SUVRs) referenced to the cerebellar cortex soon after the ratio of binding in neocortex to that in the cerebellar cortex reached an apparent steady state. Regional THK523 SUVRs were obtained for all regions sampled. Global tau burden was expressed as the average THK523 SUVR for the following cortical ROIs: frontal (consisting of the dorsolateral prefrontal, ventrolateral prefrontal and orbitofrontal regions), superior parietal, lateral temporal, lateral occipital, and anterior and posterior cingulate. Partial volume correction accounting for both GM atrophy and white-matter spillover was performed using a three-compartment approach with PMOD version 3.1 software (PMOD Technologies, Zurich, Switzerland). To establish whether either ^{18}F-florbetaben or ^{18}F-THK523 retention in the PSP patient was different from age-matched controls, a Z-score was generated for both global and regional retention. The respective Z-scores were generated against ten healthy controls who had ^{18}F-florbetaben studies and ten healthy controls who had ^{18}F-THK523 studies. Conservative Z-scores greater than 1.5, indicating just 1.5 standard deviations (SDs) from the mean of the control participants, were considered abnormal.

Results

Demographic information

The demographics of the patients whose postmortem human brain tissue was utilized for these studies, expressed as mean ± SD, are presented in Table 1. All participants assessed were of similar age with comparable postmortem intervals for tissue collection. The patient